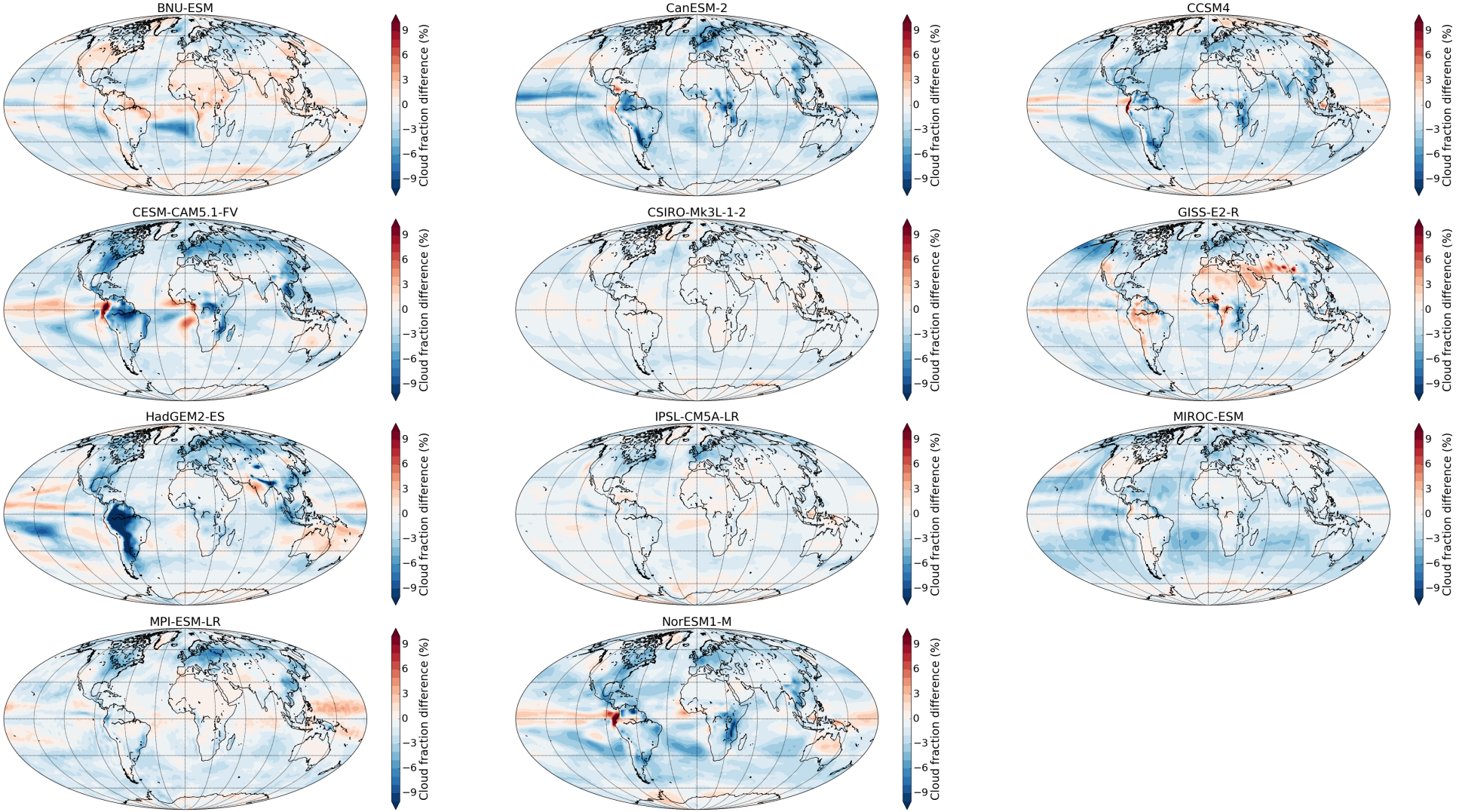

Figure S1: Change in low cloud fraction in G1 minus piControl in each model.

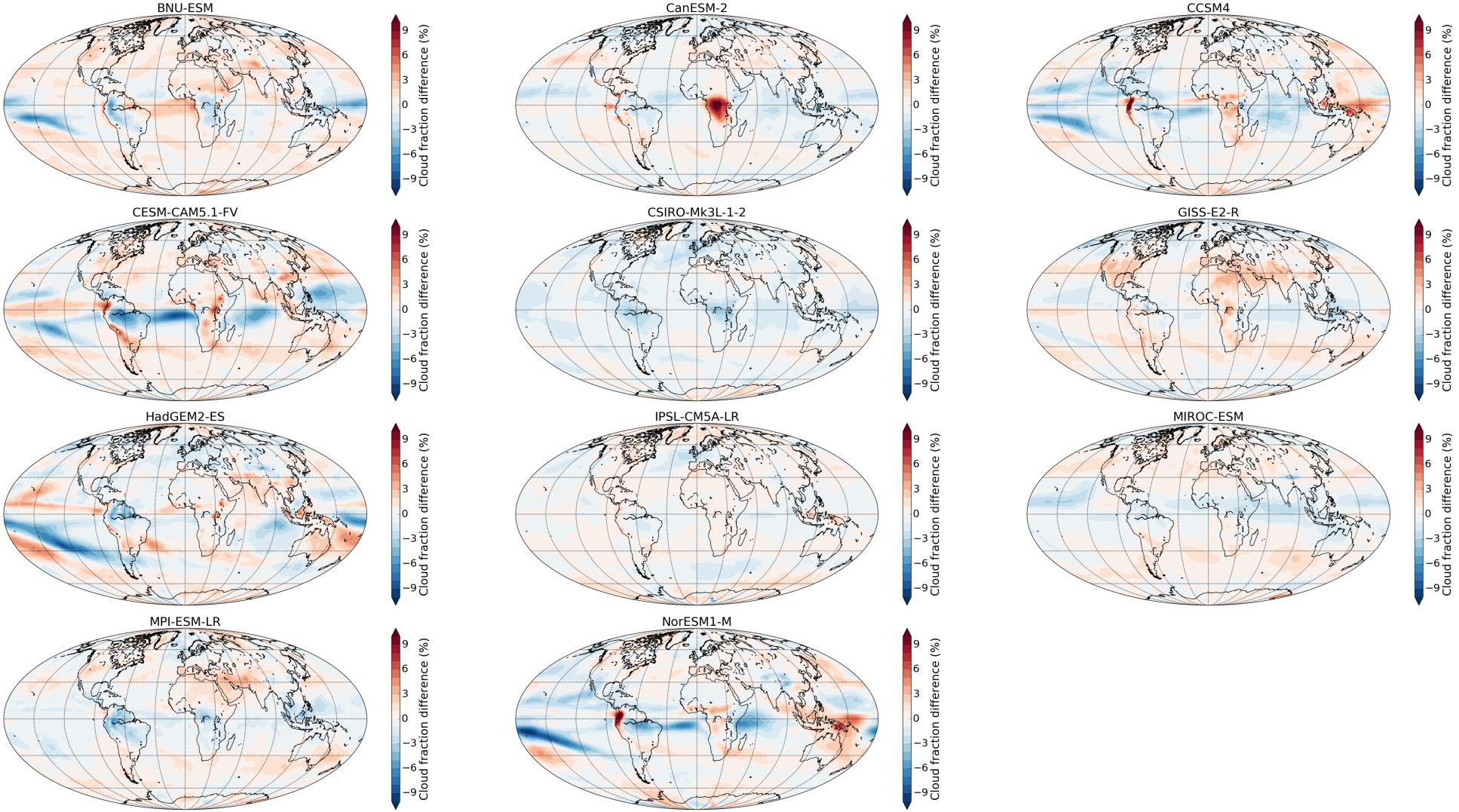

Figure S2: Change in middle cloud fraction in G1 minus piControl in each model.

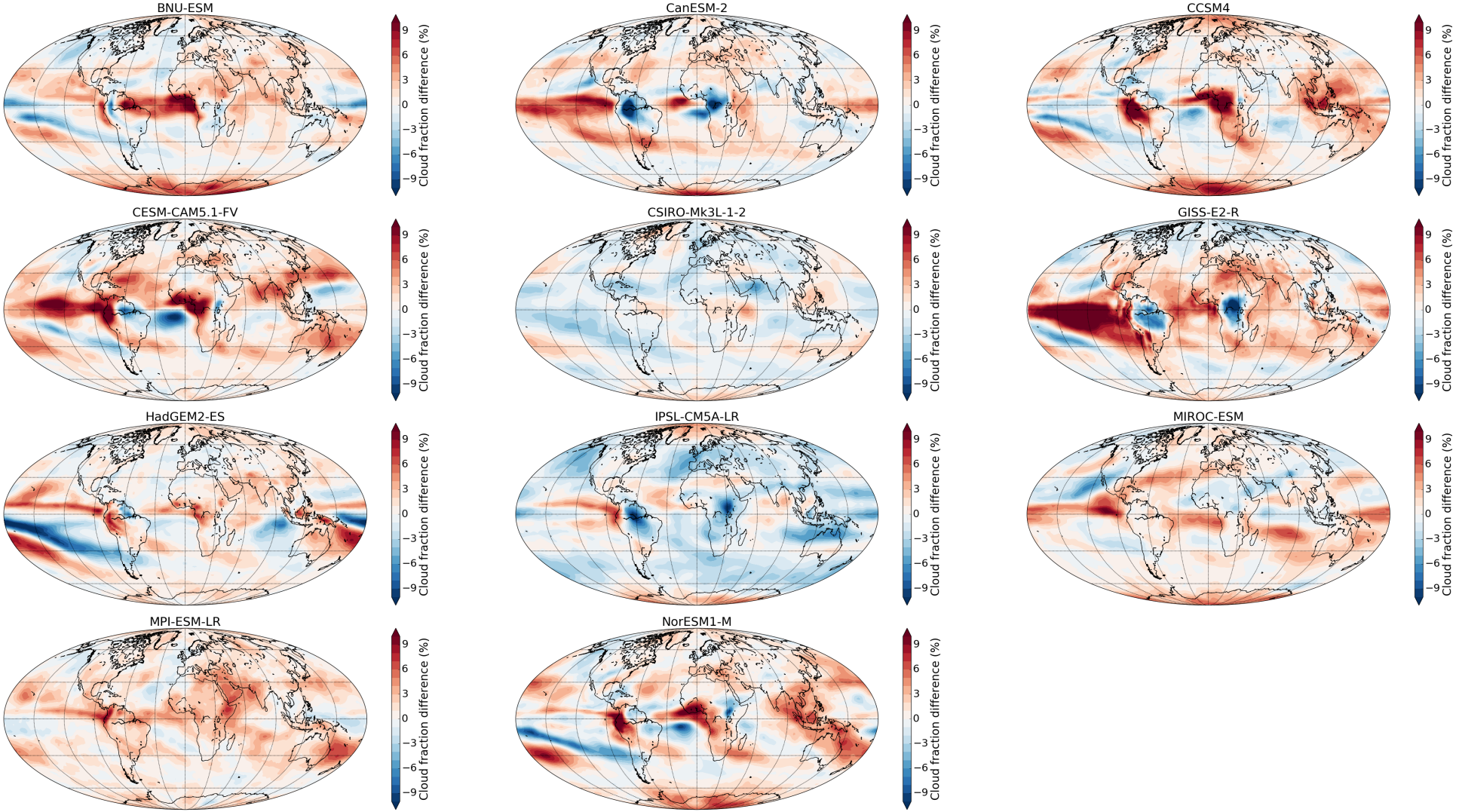

Figure S3: Change in high cloud fraction in G1 minus piControl in each model.

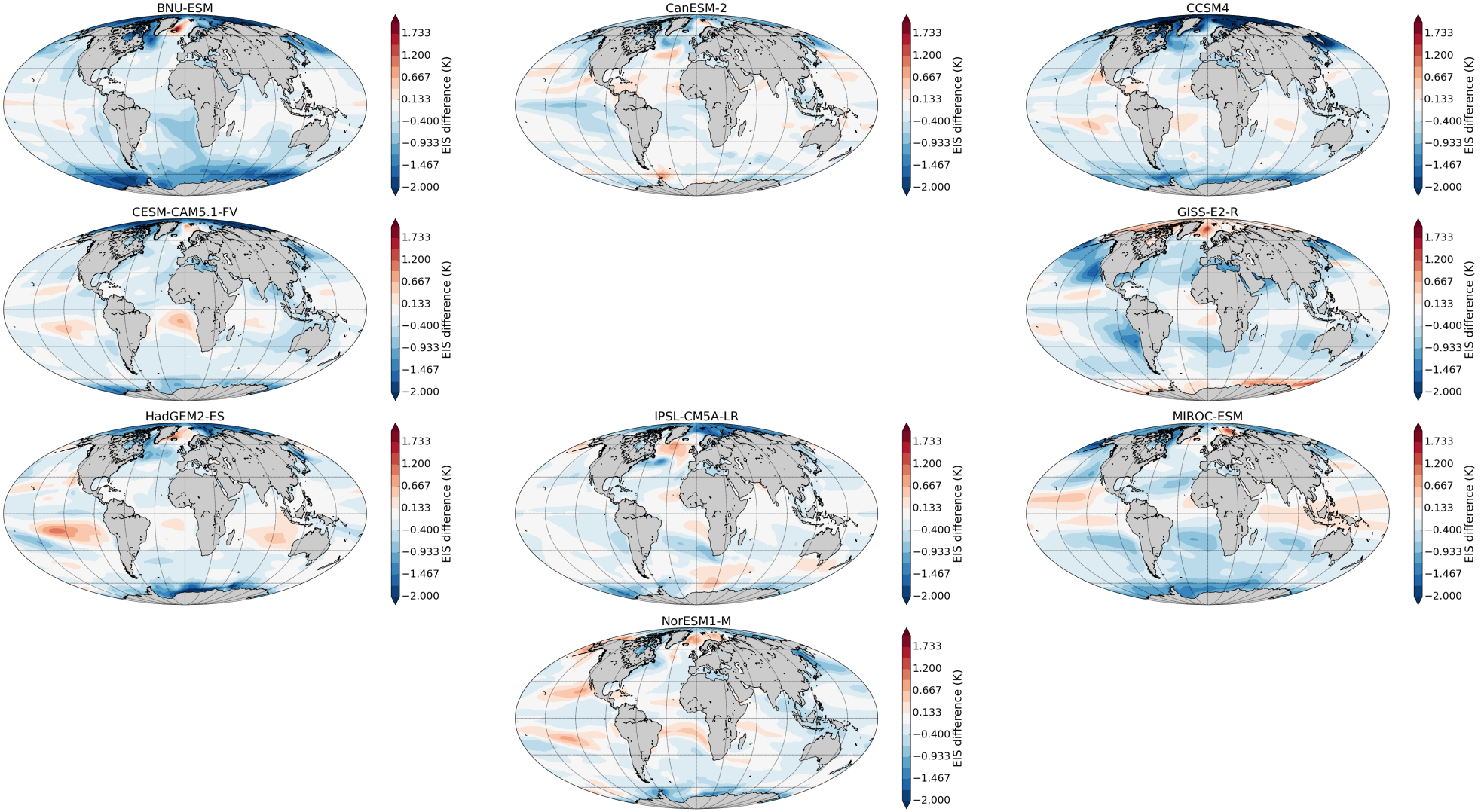

Figure S4: Change in Estimated Inversion Strength in G1 minus piControl in each model.

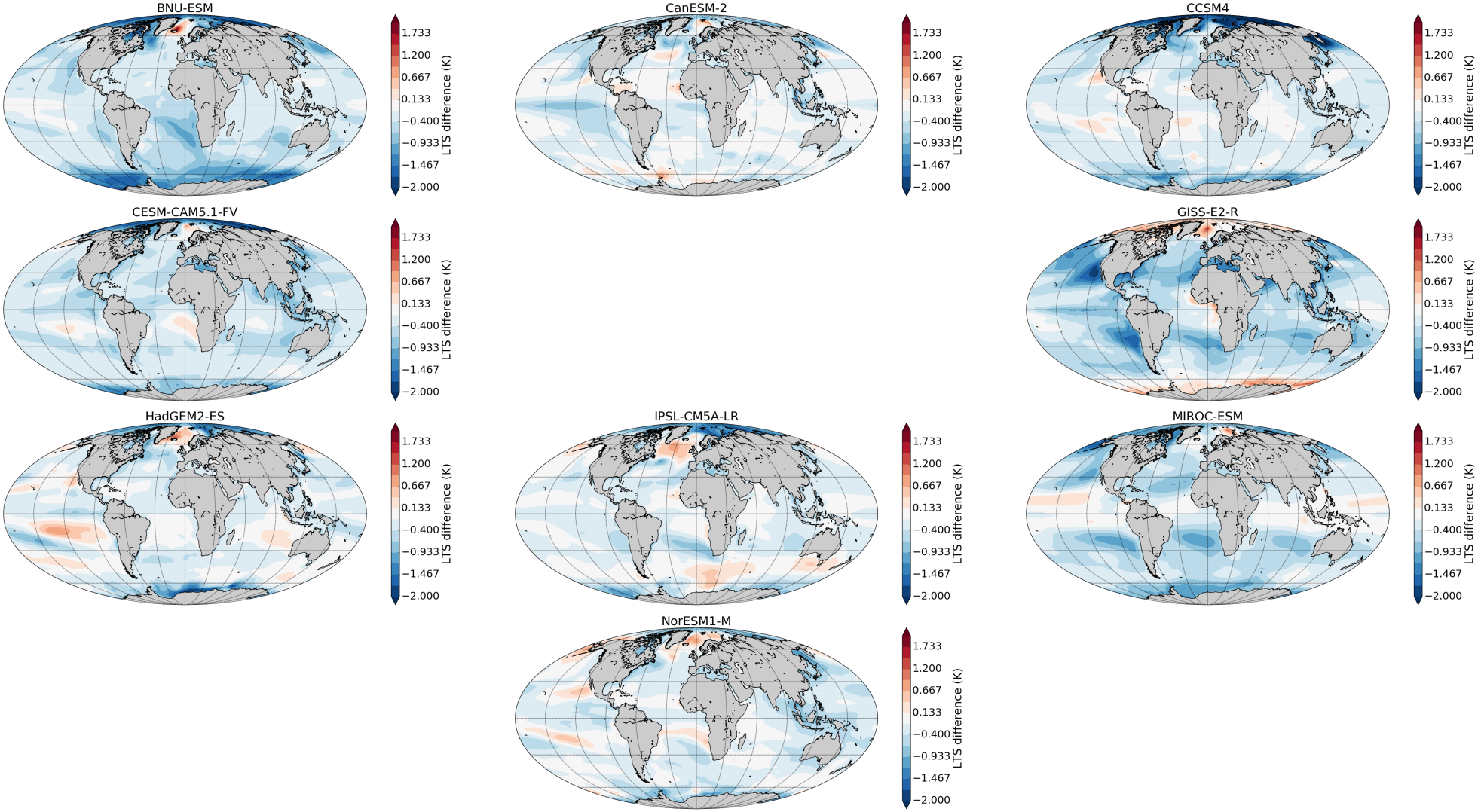

Figure S5: Change in Lower Tropospheric Stability in G1 minus piControl in each model.

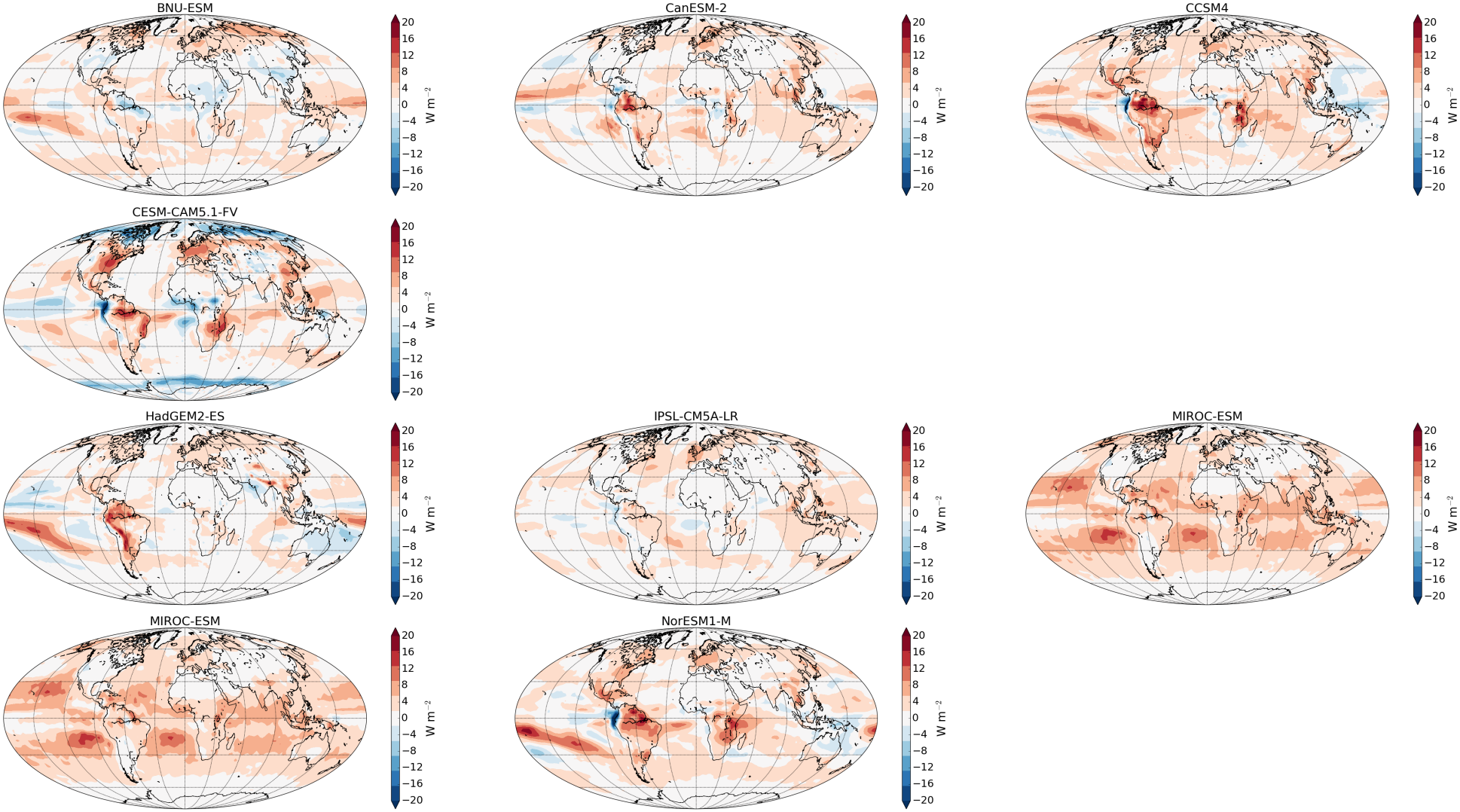

Figure S6: Change in net downward SW radiation at TOA due to changes in cloud properties, for G1 minus piControl in each model, calculated using APRP.

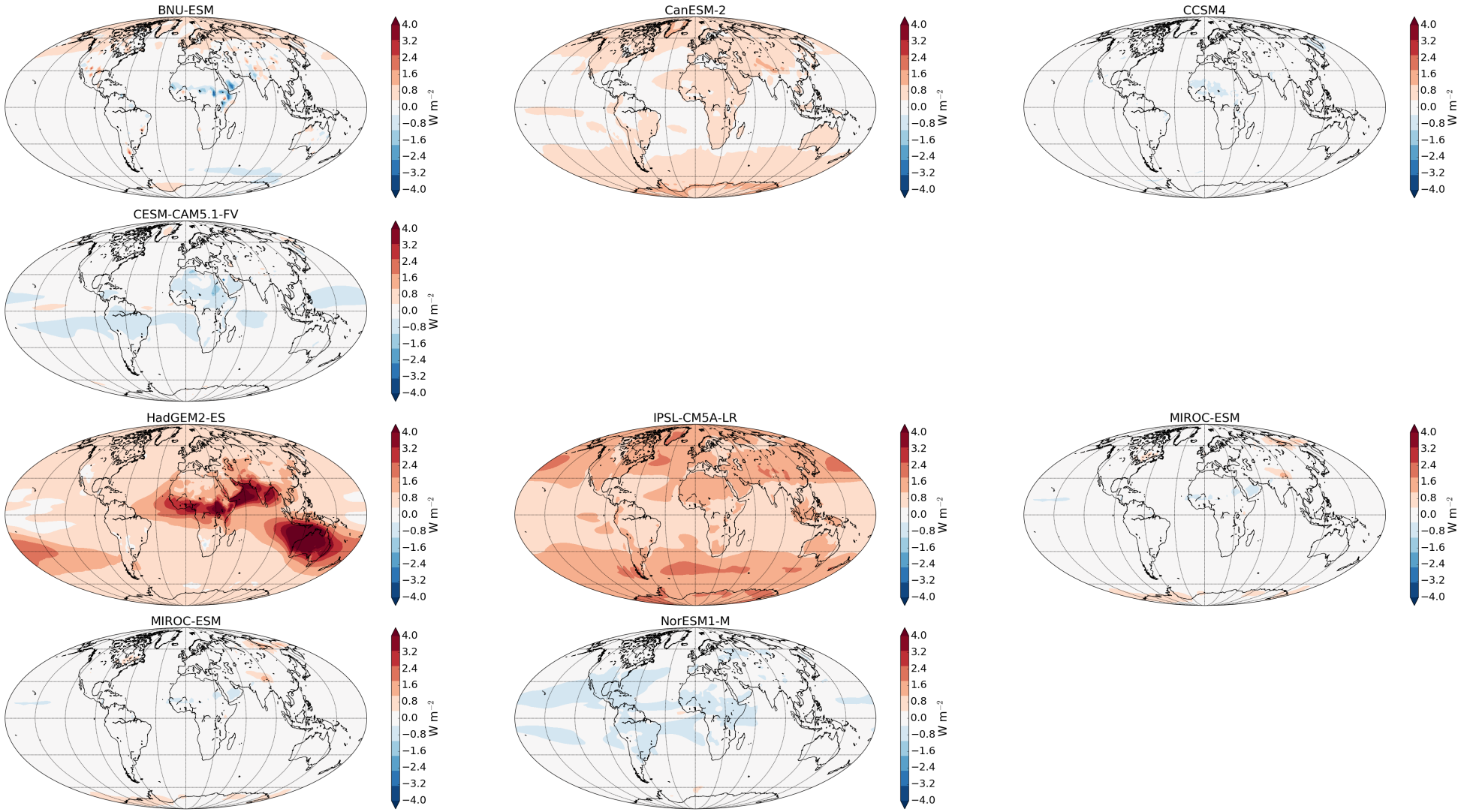

Figure S7: Change in net downward SW radiation at TOA due to changes in non-cloud atmospheric properties, for G1 minus piControl in each model, calculated using APRP.

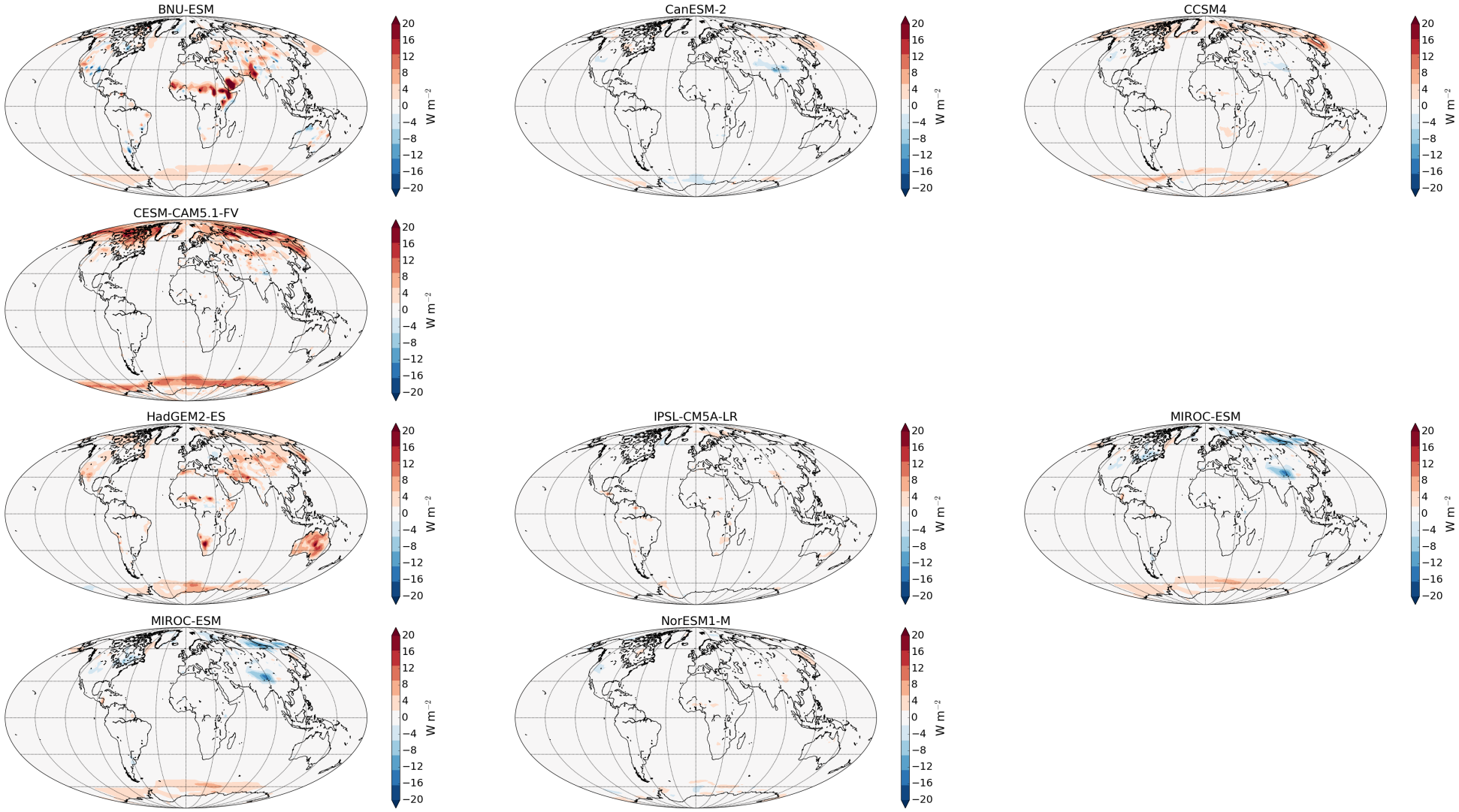

Figure S8: Change in net downward SW radiation at TOA due to changes in surface albedo, for G1 minus piControl in each model, calculated using APRP.

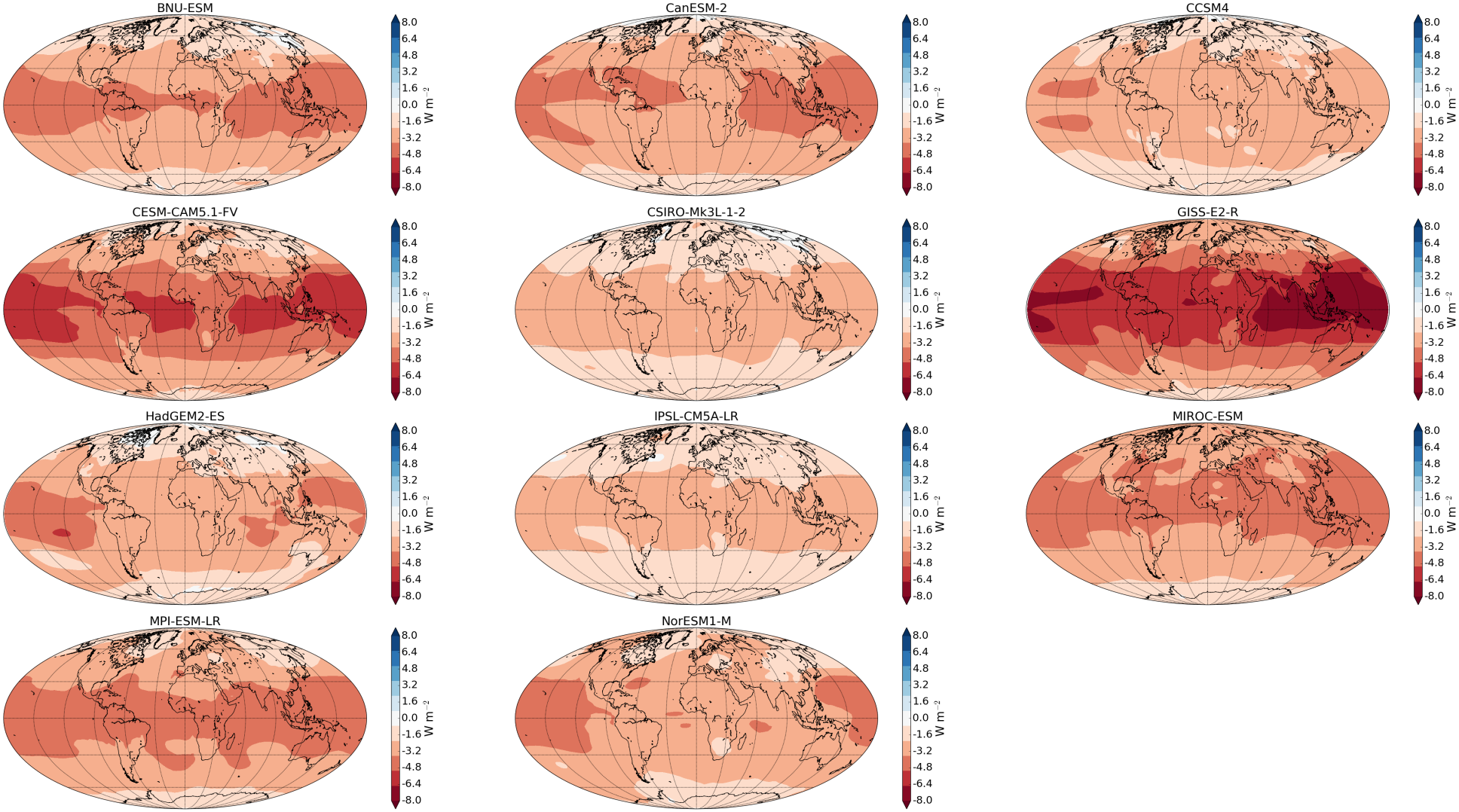

Figure S9: Change OLR due to atmospheric temperature change, calculated using radiative kernels, in G1 minus piControl in each model.

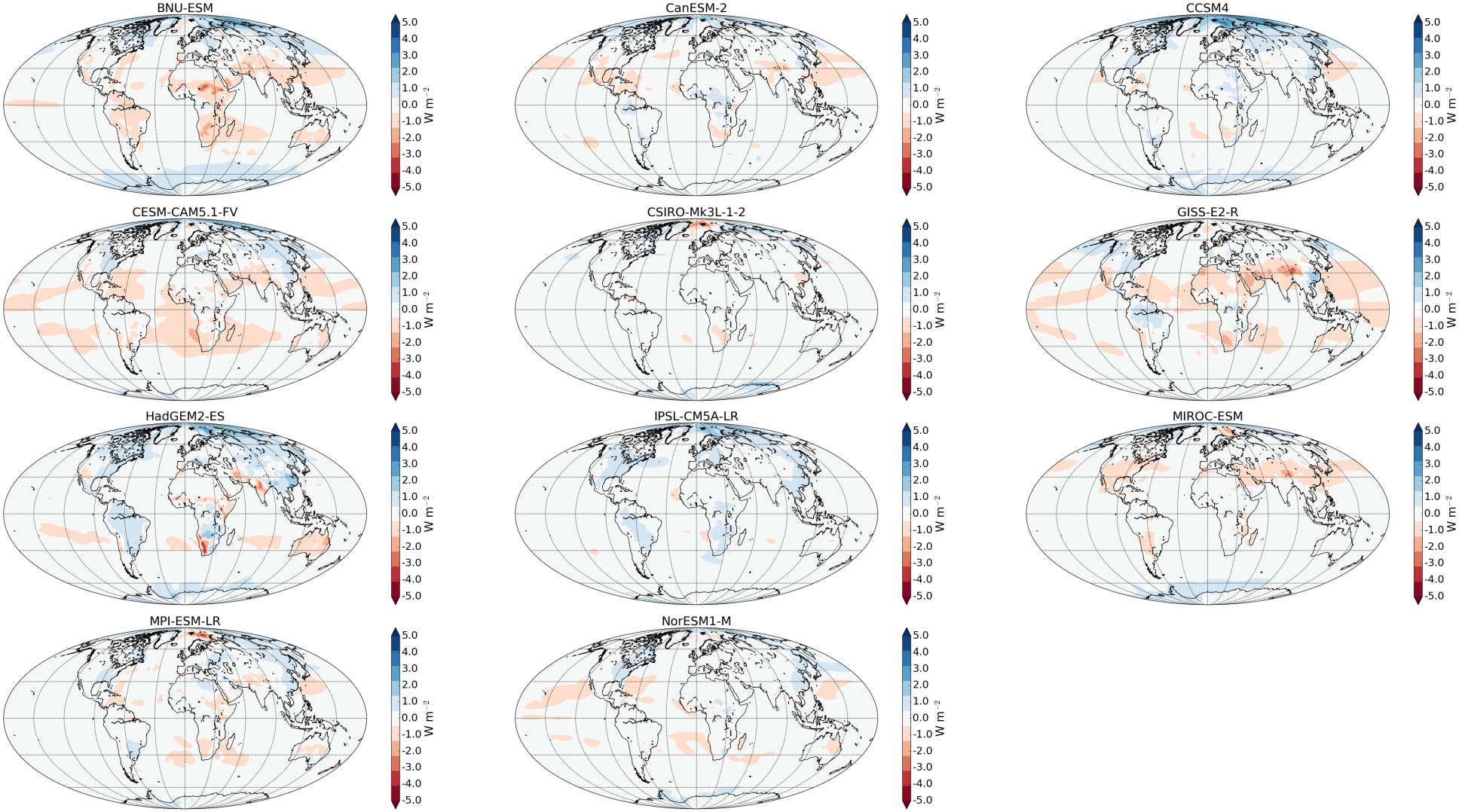

Figure S10: Change OLR due to surface temperature change, calculated using radiative kernels, in G1 minus piControl in each model.

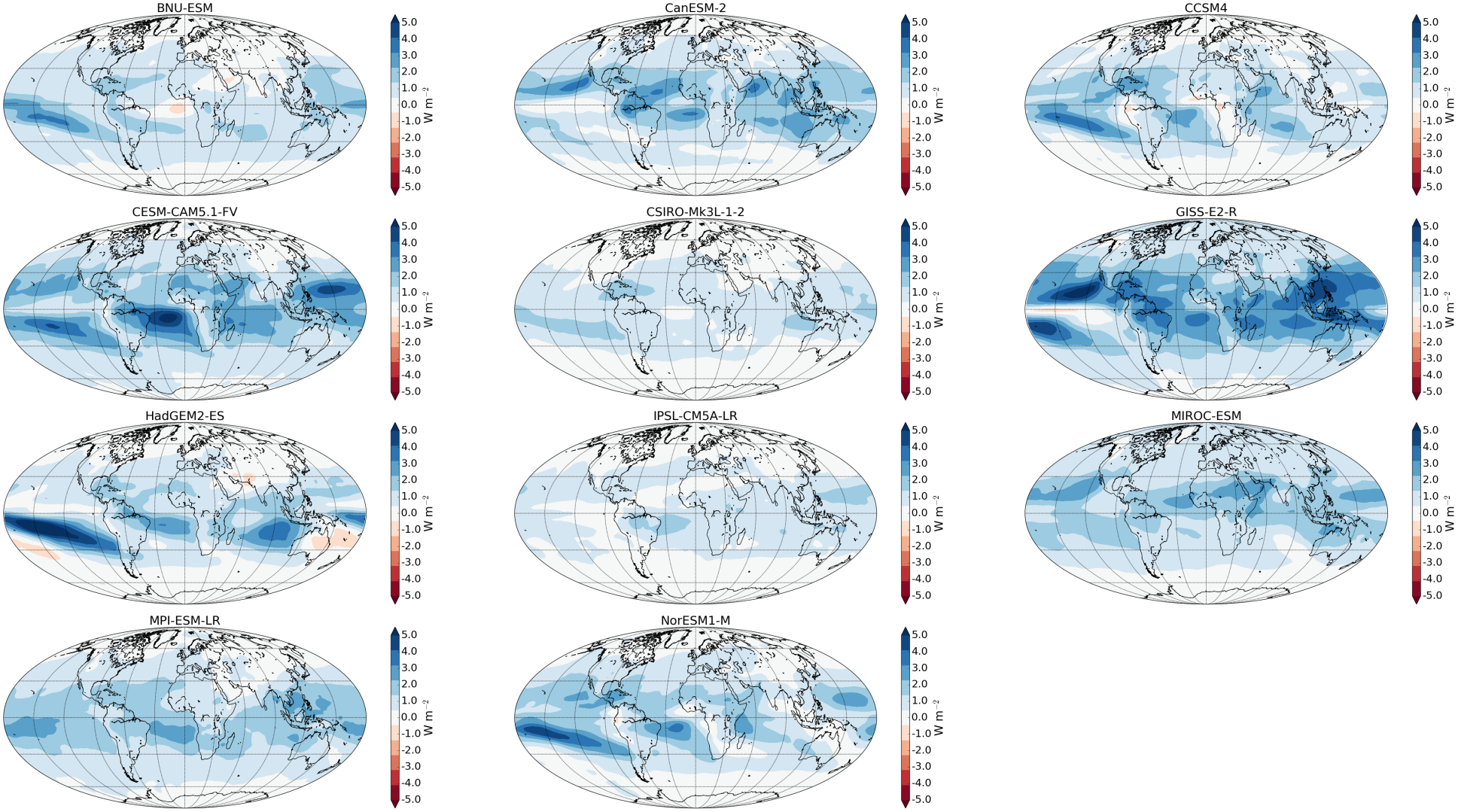

Figure S11: Change OLR due to water vapor change, calculated using radiative kernels, in G1 minus piControl in each model.

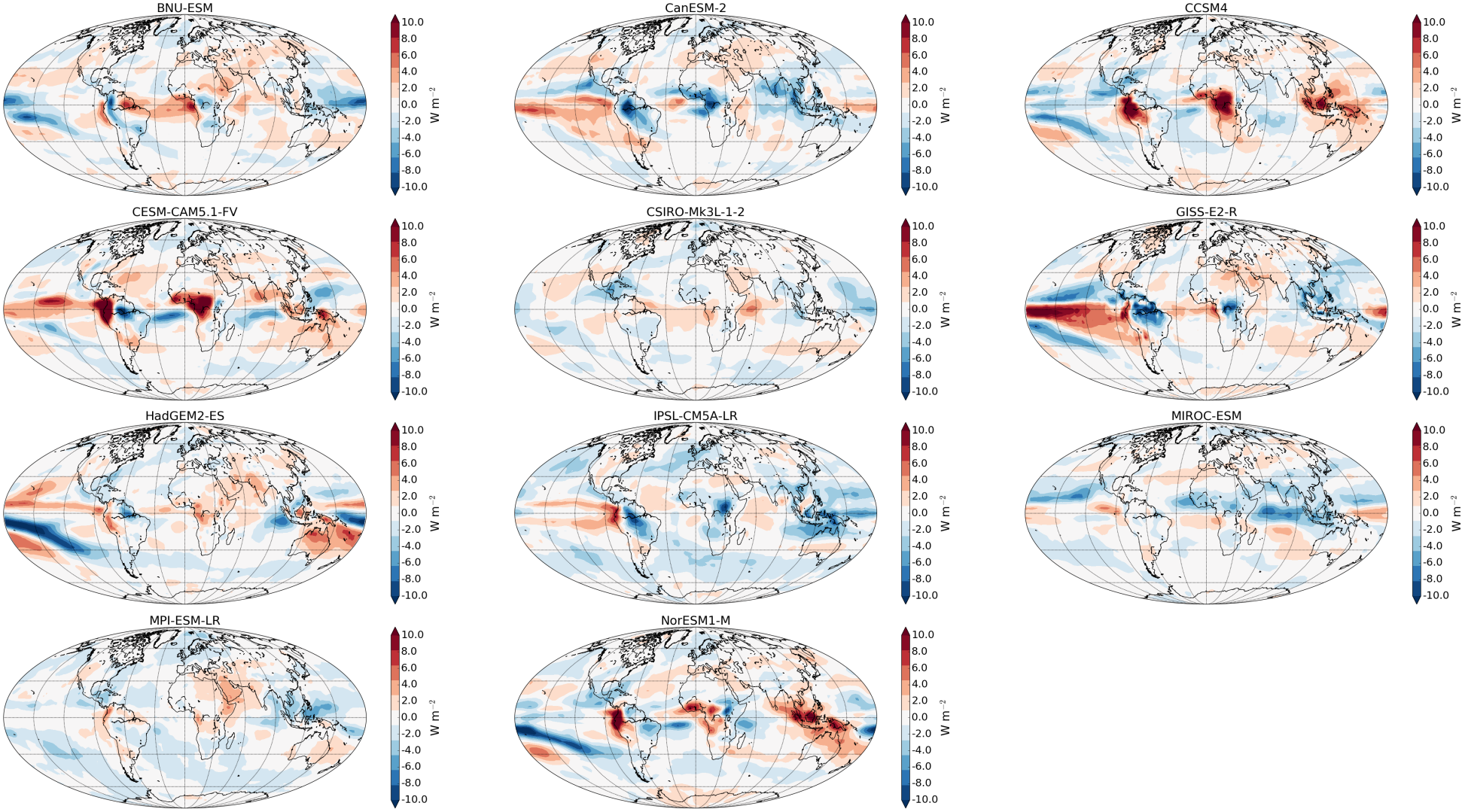

Figure S12: Change in LW cloud radiative effect, corrected for cloud masking effects using radiative kernels, in G1 minus piControl in each model.